Analysis on the Mechanism of Different Operating Conditions for DBD Plasma Excitation on Savonius VAWT

Q. Ershuai, X. Wen and W. Ying[†]

Shanghai Key Laboratory of Multiphase Flow and Heat Transfer of Power Engineering, School of Energy and Power Engineering, University of Shanghai for Science and Technology, Shanghai, 200093, China

†*Corresponding Author Email: wangying@usst.edu.cn*

ABSTRACT

Loading a dielectric barrier discharge plasma excitation on a Savonius wind turbine can improve its performance. To study the mechanism of performance improvement, the effects of three pairs of plasma excitations at different positions were comparatively studied by means of numerical simulation, and it was found that the middle position was the best for plasma excitation loading. Then, two plasma excitations in opposite directions were set at this position, and the effects were compared. The results show that plasma excitation can generate a high-velocity airflow, which can affect the velocity distribution around the blade, thereby changing the pressure distribution, and therefore the performance of the Savonius wind turbine. The effect of two opposite directions of plasma excitation loaded at the optimum position on the performance of the wind turbine varies with the change of the TSRs. When the TSR is relatively small, the influence of the two directions is very different. While the TSR is relatively large, the influence of the two directions is close.

NOMENCLATURE

A	sweeping area	k	equations of turbulent kinetic
As	aspect ratio	M	output torque
a	height of the triangular AOB	R	radius of the rotor
b	length of the triangular AOB	Δt	plasma discharge time in one excitation period
C_t	torque coefficient		
C_p	power coefficient	U	incoming wind speed
D	rotor diameter	U_0	excitation voltage
D_0	end plate diameter		
d	electrode spacing	α	charge collision efficiency factor
E	electric field intensity	δ	Dirac function
E_0	maximum electric field intensity	θ	phase angle
E_b	cut off electric field intensity on the boundary of the triangular action area	λ	tip-speed ratio
		ρ_c	charge density
e_c	electron charge constant	σ	blade thickness
F	electric field force	ω	specific consumption rate
f	frequency of applied voltage	ω_1	angular velocity
G	overlap ratio	ω_2	rotational angular velocity

1. INTRODUCTION

Energy is a precious resource prerequisite for social development (Gielen *et al*. 2019; Østergaard *et al*. 2020). Human production and life show a strong dependence on fossil energy. With the ever-increasing energy consumption, the earth's average temperature is rising rapidly, the greenhouse effect continues to intensify, and the concentration of atmospheric carbon dioxide gradually increases, which has brought a serious threat to human

civilization (Harjanne and Korhonen 2019; Mikhaylov *et al.* 2020). However, human civilization continued prosperity and development require a certain amount of energy supply. Therefore, clean and environmentally-friendly renewable energy has attracted widespread attention worldwide (Zhu *et al.* 2018).

As typical renewable energy, wind energy has allow life-cycle emissions and benefits public health and environmental protection (Veers *et al.* 2019). In the past decades of research and development, the use of wind energy has become increasingly mature, and significant progress has been made. In the past two decades, the cumulative installed capacity of wind power on a global scale has increased yearly, and large-scale wind turbines have been widely installed in the distribution network (Blaabjerg and Ma 2017). However, with the increase of large-scale wind power plants worldwide, some scholars believe this may bring some climate and environmental problems (Wang and Prinn 2011; Dai *et al.* 2015). Therefore, decentralized small wind turbines could be a sustainable choice for producing renewable energy (Tummala *et al.* 2016).

The Savonius VAWT (S-type) invented by the Finnish engineer Savonius is a classic small wind turbine driven by resistance. The Savonius wind turbine has good starting characteristics, can rotate in any direction with the wind, and can operate stably in low wind speed areas (Lee *et al.* 2016; Tahani *et al.* 2017; Belabes *et al.* 2016). However, due to the drag-driven relationship, the efficiency of the Savonius wind turbine is lower than that of the other types of wind turbines (Tummala *et al.* 2016). Thus, scholars have carried out much research on it. Under different blade helix angles, Lee *et al.* (2016) ensured that the actual wind-receiving area of the fan blades remained unchanged, and studied the changes of the power coefficient and flow pattern of the Savonius wind turbine with the helix angle. Chan *et al.* (2018) aimed at the maximum power coefficient, used the evolutionary GA to optimize the blades of the S-axis wind turbine, which increased the average power coefficient by 33%, and explained the mechanism behind the flow improvement. Kothe *et al.* (2020) investigated the aerodynamic performance of a helical Savonius rotor model by applying numerical simulation and experimental methods, where the blades are twisted of 180°. Besides, the results were compared with the two-stage S-type wind turbine with similar parameters in static torque, dynamic torque, and power coefficient. The research results suggest that although the spiral wind turbine manufacturing process is more complicated, its torque is more stable with a higher power coefficient. Tahani *et al* (2017) modeled an innovative Savonis wind turbine designed for building ventilation and power supply problems. A twisted wind turbine with a tapered shaft and a variable cross-section wind turbine are proposed. Besides, through numerical simulation, it is inferred that the conical shaft twisted wind turbine has better aerodynamic performance. Bethi *et al.* (2019) placed the S-type wind turbine next to the steady train in the train tunnel. They numerically verified the practical relevance of S-type wind turbines for collecting wind energy in unstable and high-speed wind currents generated by trains. Because the traditional S-type wind turbine cannot collect energy under this working condition, they proposed a new design that can collect energy and generate power without affecting the efficiency of train travel and evaluated it.

The active flow control technology is considered as a way to reduce the cost of wind energy (Cooney *et al.* 2016), and has been widely used in aerodynamics (Shmilovich *et al.* 2016; Lin *et al.* 2016). Among them, the plasma flow control technology can commonly be used to control boundary layer, delay dynamic stall, restrain flow separation, reduce drag and increase lift (Li *et al.* 2019; Adamiak 2020). Usually, according to the discharging principle and plasma characteristics, plasma excitation can be divided into arc discharge, dielectric barrier discharge (DBD), nanosecond pulse discharge, and other excitation types (Li and Wu 2020). As a relatively novel flow control technology. By applying a sufficiently high AC voltage to the electrodes, the DBD plasma active flow control technology can accelerate the fluid near the driver and provide momentum (Abdollahzadeh *et al.* 2018; Yang *et al.* 2016).

The dielectric barrier discharge plasma has received extensive attention from scholars since it can control the large global flow by local and small airflow disturbances (Chen *et al.* 2020). Baleriola *et al.* (2016) realized the loop control strategy, where three sets of multi-dielectric barrier discharge plasma drivers at different positions are arranged on the wind turbine wing with a circular trailing edge. In this way, the aerodynamic load fluctuation on the blade was reduced, and the effectiveness of control through load and pressure measurement was shown. In the small horizontal axis wind turbine rotation experiment, Jukes (2015) characterized and evaluated the control of the plasma driver on the stall characteristics. The research results show that generated by the plasma driver placed along the span, the chordal volume force presents little effect on the flow separation. The plasma driver along the blade chord generates a radial volume force, which successfully reduces the rotational stall. Pescini *et al.* (2017) evaluated the control potential of the DBD plasma driver for separation flow by studying the characteristics of the boundary layer at low Reynolds numbers. The results show that there is a large countercurrent and high turbulence intensity in the separation zone in the case of no drive. However, the driving of the plasma reduces the separation zone, flow angle, and turbulence intensity. Vernet *et al.* (2015) verified the ability of the DBD plasma driver to delay flow separation and reduce drag by studying the flow around a half-cylinder under the action of a turbulent boundary layer. Moreover, the drag reduction effect was optimized through the parameterized study of the position and driving voltage of the drivers. Mazaheri *et al.* (2016) proposed an improved phenomenological model to simulate the effect of the DBD plasma driver on the aerodynamic performance of the DU 91-W2-250 airfoil. It is found that when the DBD driver is

installed in the middle, the lift coefficient is increased by 70.1%. The lift-to-drag ratio is increased by more than 550%. Lombardi *et al.* (2013) proposed a closed-loop plasma drive control scheme and applied it to a periodically oscillating airfoil. In the light stall state, the comprehensive lift of one cycle is increased by 12%, and the maximum pitching moment is reduced by 60%. In order to improve the aerodynamic performance of the NACA 0015 airfoil, Wong *et al.* (2020) conducted an experimental study on a novel sawtooth DBD plasma actuator. When the airfoil was Re=7.7$\times$10^4, the stall angle was delayed by 6°, and the maximum lift coefficient was increased by 28.6%.

The resistance difference between the blade two sides drives the Savonius VAWT to rotate and do work. However, the resistance caused by the impact of the airflow on the convex surface will hinder the workmanship. In contrast, DBD plasma excitation can affect the boundary layer. In order to reduce the resistance of the airflow on the convex surface, DBD plasma excitation is added on this side, hoping to improve the wind turbine's function. Firstly, we studied the effect of the installation position on the torque coefficient. Secondly, the velocity and pressure fields around the blades are analyzed in detail to explain the variation in wind turbine performance. Finally, in the most suitable installation position, two plasma excitations in opposite directions were loaded, and their effects were compared.

2. CALCULATION MODEL

2.1 Geometric Model

This paper chooses the 2D Savonius VAWT as the study object (Fujisawa and Gotoh 1994), as shown in Fig. 1, where the overlap ratio G=0.15, the rotor diameter D=300mm, the blade thickness σ=4mm, the end plate diameter D_0=1.1D and the aspect ratio As=1. At the incident wind speed U=6m/s, the tip-speed ratio λ value range between 0.233 and 1.3. The wind turbine rotates counterclockwise around the center of the rotor with an angular velocity ω_1. At the initial moment, the phase angle θ is 0°.
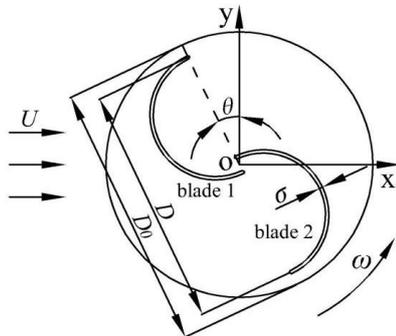

Fig. 1. Structure of Savonius VAWT.

To generate fully developed flows, the computational domain of the model is now designed as a rectangular area, as shown in Fig. 2, with a size of 100D_0×60D_0.
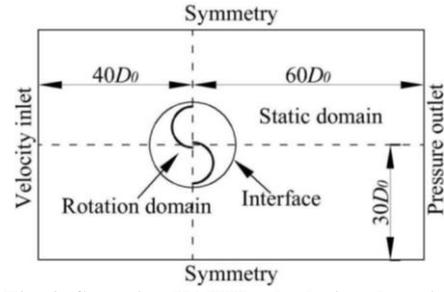

Fig. 2. Savonius VAWT calculation domain.

The boundary conditions are set to speed inlet, and pressure outlet, and the upper and lower sides are symmetrical boundaries. The surface of the blade is a non-slip wall. Sliding meshes are the most accurate method of simulating the flow field against a moving reference system and are suitable for periodic unsteady problems. Therefore, the rotation of the wind turbine is simulated using a sliding mesh. The computational domain includes two domains: the rotating domain on the inside and the stationary domain on the outside, and their overlapping boundary is set to the slip interface.

2.2 Plasma Excitation Model

The phenomenological model put forward by Shyy *et al.* (2002) is used. As shown in Fig. 3, the triangle AOB represents the area of action of the model, and in order to make the model easier to understand, the electric field force is replaced by the body force. In this region, to simplify the model, the electric field force is assumed to be linearly distributed and parallel to the AB side and has a maximum value at point O. Under the action of the spatially inhomogeneous electric field, the electrons move in the opposite direction of the electric field, and the positive ions move in the direction of the electric field, in which the electron momentum is much smaller than the ion momentum, and the momentum exchange can be neglected. The ions collide with neutral gas molecules in moving with the direction of the electric field gradient (Nie *et al.* 2012), thereby exchanging momentum. As a result, a jet can be generated from the OA edge.

The electric field intensity E distribution is:

$$E = E_0 - k_1 x - k_2 y \qquad (1)$$

$$E_0 = U_0/d \qquad (2)$$

where U_0, E_0, and d are the excitation voltage, the maximum electric field intensity and the electrode spacing, respectively.

With linearly distributed electric field force, then

$$k_1 = (E_0 - E_b)/b \qquad (3)$$

$$k_2 = (E_0 - E_b)/a \qquad (4)$$

where E_b is the cut-off electric field strength; b is the length of OB; a is the length of OA .

In the area, the electric field force F distribution is:

$$F = f\alpha\rho_c e_c \Delta t E \delta \qquad (5)$$

where δ is the Dirac function; f is the frequency of applied voltage; Δt is the plasma discharge time in one excitation period; α is the charge collision efficiency factor; e_c is the electron charge constant; ρ_c is the charge density.

a=0.01m and b=0.02m are the parameter settings of the plasma excitation in this paper. The charge density is $1\times10^{11}C/cm^3$, the electron charge constant is 1.602×10^{-19}, the discharge time is 67μs, the electric field boundary cut-off voltage is 30kV/cm, the electrode spacing is 0.25mm, the excitation voltage is 6000V, and the voltage frequency is 1000Hz. The corresponding momentum source term is added for the Navier-Stokes equation. In this way, the plasma exciter in the simulation will caused the volume force with a control effect. The UDF is adopted to load volume force with plasma excitation.
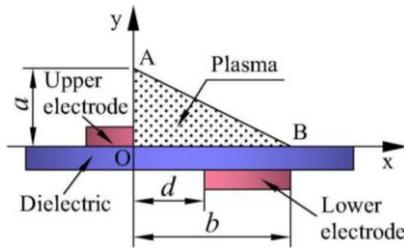

Fig. 3. Simplified model of plasma excitation.

3. NUMERICAL CALCULATION AND VERIFICATION

3.1 Meshing and Turbulence Model

A structured mesh is adopted in the blade boundary layer during the meshing process, which has better mesh quality. To satisfy $Y^+<1$, the first layer is set to 4.9×10^{-5} as the grid height. For a single blade, the number of nodes is 495 on the surface. The central rotor area uses an unstructured grid, and the rest uses a structured grid. The unstructured grid uses triangular mesh. Totally, the number of grids is about 100,000. The overall computational domain grid and the central rotation area grid are shown in Figs 4 and 5.

The finite volume method is applied to discretize the control equations in ANSYS Fluent. As a very popular eddy current-viscosity model, the SST k-ω model has the advantages of both the free flow k-ε model and the boundary layer flow k-ω model and has a good performance in the stability and reliability of the solution. Chan *et al.* (2018), Kothe *et al.* (2020), and Tahani *et al* (2017) all used this model to conduct numerical simulations of Savonius vertical axis wind turbines. To accurately simulate the rotation of the wind turbine, the *SST k-ω* turbulence model, a two-equation eddy viscosity model, is used in this paper.

3.2 Performance Calculation

The second-order upwind style is adopted in the equation of the turbulent kinetic energy K to obtain more accurate calculation results, as well as the specific consumption rate ω. The pressure implicit
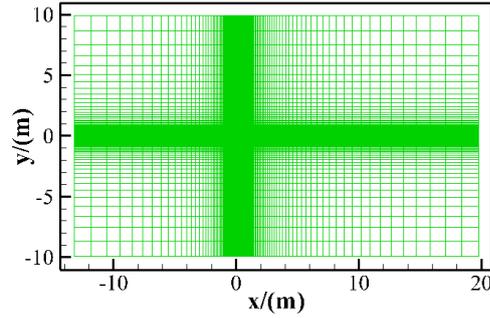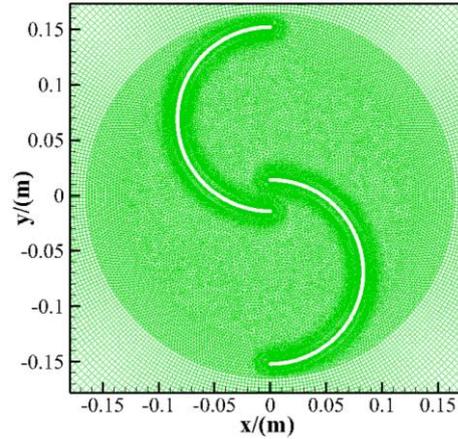

Fig. 4. Computational domain grid.

Fig. 5. Rotating area grid.

operator is used to split the pressure correction algorithm and the PISO velocity in the calculation process. In the simulation, the wind turbine model was simplified, and only the blades were retained without considering the central rotation axis and the support.

The tip speed ratio (TSR), torque coefficient, and power coefficient are defined as follows:

$$\lambda = \omega R/U \tag{6}$$

$$C_t = M/(1/2\rho U^2 AR) \tag{7}$$

$$C_p = M\omega/(1/2\rho U^3 A) \tag{8}$$

where λ is the TSR; ω is the rotational angular velocity; C_t is the torque coefficient; M is the output torque; R is the radius of the rotor; U is the incoming wind speed; A is the sweeping area; C_p is the power coefficient.

3.3 Independence Verification and Model Verification

The independence of the grid needs to be verified by the boundary as mentioned above conditions and calculation methods. Three sets of grids including 100,000, 210,000 and 350,000 are constructed. The calculated torque coefficient error between 100,000 and 210,000 grids is 0.58%, and the error with 350,000 grids is 0.4%, with the TSR λ=0.992. It shows that the requirements of calculation accuracy are met when the number of grids reaches 100,000, so there is no need for further refinements of the grid. Therefore, to avoid unnecessary calculations and

reduce computing costs, 100,000 grids is chosen to perform subsequent calculations in this paper.

In addition, three groups of time steps, 360, 720 and 1080 were selected, and their independence was verified. After the calculation converges, the torque coefficient values are obtained accordingly. The torque coefficient error between 720 and 1080 steps is less than 0.1%. Thus, a cycle of 720 time steps will be applied for the following simulation.

Moreover, the power coefficient selected in this article under different TSRs is calculated. Moreover, the same comparison results between the computed results and experimental data is presented in Fig. 6 (Fujisawa and Gotoh 1994). Because the wind turbine model in the numerical simulation is simplified, without considering the central rotation axis and the support, the power coefficient obtained by the calculation is larger than the experiment results. The positions of the optimum TSRs in the numerical simulation and experiment are around 0.992. Therefore, the simulation method is believed to be reliable and can present relatively good results.
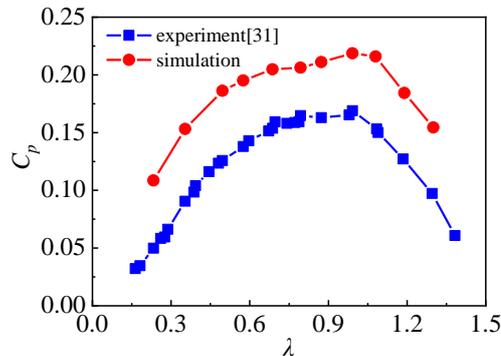

Fig. 6. Comparison of power coefficient variation curves.

4. ANALYSIS AND DISCUSSION

Figure 7 is a schematic diagram of the installation positions. There are three pairs of plasma exciters, including Pos_1&Pos_6, Pos_2&Pos_5 and Pos_3&Pos_4, which are the first, second and third pair. Besides, 1000Hz is chosen as the voltage excitation frequency in the model. The plasma exciters are set at the above positions separately, and their effects on the torque coefficients with different TSRs, including 0.233, 0.794, and 1.080 is studied.

4.1 Analysis plasma excitation effect of Pos_1&Pos_6

In Fig. 9, when plasma excitation is placed in the blades Pos_1&Pos_6, the low-speed area on the windward side is slightly reduced. However, the high-speed airflow appearing at the outermost ends of the two blades has a more significant impact on the leeward side. When λ=0.233, the airflow on the concave surface of blade 1 is hindered by the high-speed airflow excited by the plasma. In the region far from the rotation center, the airflow velocity decreases and the pressure rises, thereby increasing
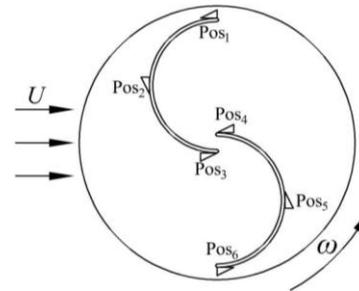

Fig. 7. Schematic diagram of the installation position of the plasma exciter.

the pressure that promotes the rotation of the blade. At the same time, the pressure on the windward surface of the blade 2 is increased, and the pressure on the leeward surface is decreased. This makes the difference of positive pressure increase and promotes the rotation. That is, the wind resistance on blade 2 increases. The plasma excitation increases the resistance difference between the two blades under this operating condition. However, due to the small TSR, the incoming flow passes through the center of the wind turbine. Air jets are formed between the original wind turbine blades and perform work on the blade 1 concave surface. The application of plasma excitation suppresses the jet. It causes a loss of practical work. Therefore, the wind turbine's overall performance is slightly reduced.

If the TSR is 0.794, the airflow with high-speed driven by the plasma excitation greatly decreases the pressure of the outermost ends of the two blades on the convex side. At this time, for blade 1, its concave surface pressure increases, and the high-pressure area of the convex surface is significantly reduced, which increases the pressure that promotes the rotation of the blade and reduces the pressure that hinders the rotation, so the output torque increases. Due to the reduction of the concave pressure, although the forward pressure difference of the blade 2 is reduced, the reduction is small. In general, the plasma excitation under this working condition promotes the wind turbine overall performance.

4.2 Analysis for plasma excitation effect of Pos_2&Pos_5

The plasma excitation is added at Pos_2&Pos_5, As shown in Fig. 9. Whether it is a small TSR or a large TSR, the blade convex side produces a wide range of high-speed flowing airflow. When the TSR=0.233, the reason for the large increase in the torque coefficient, as shown in Fig. 11, is mainly because the pressure of the blade 2 on the concave side has been significantly increased under the action of plasma excitation. The originally small positive differential pressure was significantly enhanced, while the negative differential pressure was reduced, which greatly facilitated the rotation. At this time, for blade 1, the positive pressure difference that promotes the rotation also increases slightly. They work together to increase the output torque and enhance the power.

If the TSR=0.794, on the blade 2 concave side, although the plasma excitation did not cause the
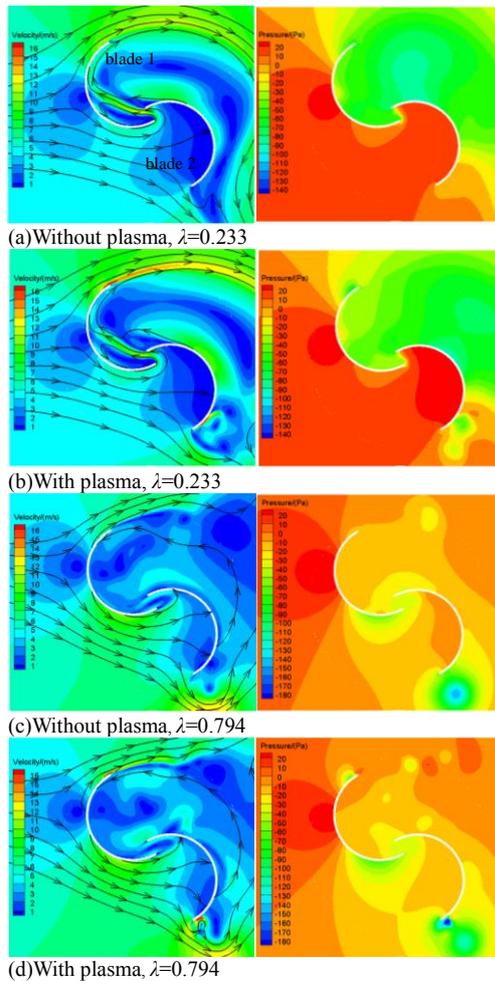
(a)Without plasma, λ=0.233

(b)With plasma, λ=0.233

(c)Without plasma, λ=0.794

(d)With plasma, λ=0.794

Fig. 8. Comparison before and after adding plasma excitation at positions Pos₁&Pos₆.

(a)Without plasma, λ=0.233

(b)With plasma, λ=0.233

(c)Without plasma, λ=0.794

(d)With plasma, λ=0.794

Fig. 9. Comparison before and after adding plasma excitation at positions Pos₂&Pos₅

pressure to exceed its convex side, the pressure difference between these two sides is significantly decreased. This reduces the negative pressure differential across the vanes 2, weakening the impediment to rotation. At this time, the pressure around the blade 1 does not change significantly. Overall, the output torque of the wind turbine increases.

4.3 Analysis for Plasma Excitation Effect of Pos₃&Pos₄

If the TSR is 0.233, due to the plasma excitation, high-speed airflow is generated at positions Pos3&Pos4 and continuously passes through the center of rotation. This essentially hinders the flow of free flow. It can be seen from the velocity cloud diagram in Fig. 10 that the air velocity near the plasma excitation increases significantly. However, since the location where the excitation is applied is close to the wind turbine shaft, the generated torque is short. Besides, the induced high-speed airflow increases the wind turbine torque to a small extent, and the excitation effect suppresses the original air jet between the two blades at that moment. This causes a significant reduction in the torque generated on the blade 1, reducing the wind turbine overall performance.
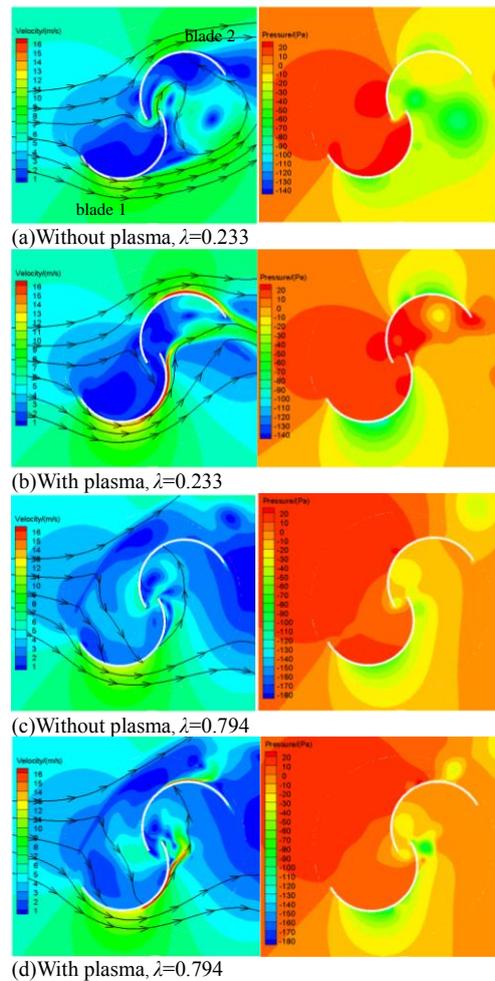
If the TSR=0.794. It can be seen from the velocity cloud graph that the air jet formed between the two blades is small. It does minor work on blade 1. So, after applying plasma excitation, this part of the energy will not be lost. Meanwhile, plasma excitation's high-speed air flow does not completely pass through the wind turbine rotation center. To a certain extent, the positive pressure difference is increased between the two sides of blade 2, and the wind turbine performance is enhanced. However, for blade 1, the pressure on the concave surface is reduced, and the pressure on the convex surface is basically unchanged. Thus, the negative pressure difference increases, which offsets the positive pressure difference generated by a part of the blade 2. Under this working condition, the wind turbine torque coefficient slightly increased. In summary, the aerodynamic performance of the S-type VAWT can be also maximized while applying a plasma exciter at Pos₂&Pos₅.

4.4 Comparison of Plasma Excitation Effects at Different Positions

In Fig. 11, the TSR increases as the torque coefficient decreases. When λ=0.233, Plasma excitation at positions Pos1&Pos6 reduces torque coefficient slightly; the torque coefficient decreases
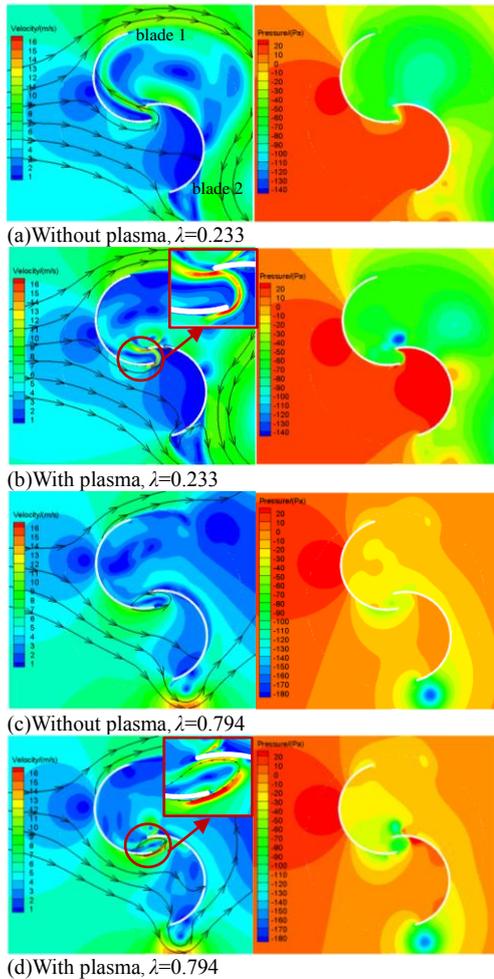
(a)Without plasma, λ=0.233

(b)With plasma, λ=0.233

(c)Without plasma, λ=0.794

(d)With plasma, λ=0.794

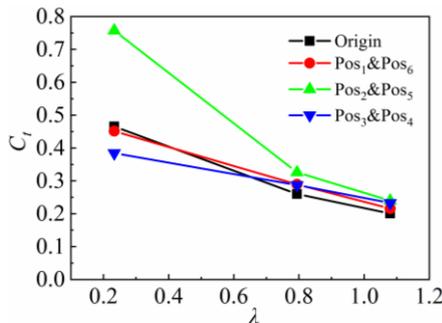**Fig. 10. Comparison without and with adding plasma excitation at positions Pos$_3$&Pos$_4$.**

Fig. 11. Torque coefficients of wind turbine under different excitation positions.

significantly with adding plasma excitation at Pos$_3$&Pos$_4$. However, Pos$_2$&Pos$_5$ can dramatically improve the torque coefficient. When the TSR are 0.794 and 1.080, the torque coefficient grows up for all these three pairs of excitation positions. When λ=0.794, the second pair shows the best effect, while the first and the third pair are close. When λ=1.080, Pos$_2$&Pos$_5$ shows the best result, while Pos$_1$&Pos$_6$ is the worst.

The main reason for the above phenomenon is that after the plasma excitation is set, the fluid around the blade is disturbed since the action of the volume force. The flow field velocity around the blade

changes, which affects the distribution of pressure field around the blade. Fig. 8 to Fig. 10 show the distribution of velocity and pressure around the blades before and after plasma excitation is installed at different positions, and the moment when the excitation effect is most obvious is selected for comparative analysis. Since plasma excitation has a similar impact on wind turbines with TSRs of 0.794 and 1.080, a working condition of 0.794 for the primary analysis in the two TSRs is chosen. Furthermore, adding plasma excitation will generate high-speed airflow at the corresponding position. Moreover, it's more obvious under the small TSR. This is because the speed is slower when the wind turbine is at a small TSR. The air velocity around the blades is small. It is easier to be disturbed under the same volume force.

4.5 Analysis of the Effect of Electric Field Forces in Different Directions

A plasma exciter is installed in the middle of the Savonius wind turbine blade with a different electric field force direction. As shown in Fig. 12, these are denoted as Pos$_2$'&Pos$_5$'. Besides, the numerical simulation research is conducted when the TSR equals 0.233, 0.794 and 1.080. Direction A is for the installation position of Pos$_2$&Pos$_5$, while Direction B is for the installation position of Pos$_2$'&Pos$_5$'. Fig. 13 shows the specific calculation results. When TSR=0.233, compared with Direction B, Direction A shows better effect. When TSR equals 0.794 and 1.080, in both Direction A and Direction B, electric field forces' enhanced effect on the torque coefficient, and the enhancement effect of both directions is relatively close.
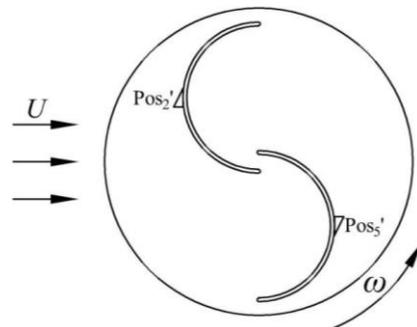

Fig. 12. Schematic diagram of the plasma exciter after changing its direction.
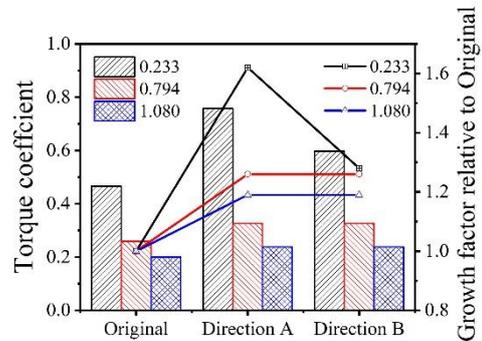

Fig. 13. Torque coefficient and its growth factor under the distribution of electric field force in different directions.

To analyze the causes of the above phenomenon, the time when the excitation effect is most apparent in one rotation period after the calculation converges (the time shown in Fig. 9) is taken. The blade surface pressure coefficients were compared with and without the addition of two pairs of plasma excitations in opposite directions. (Fig. 14 and Fig. 15). In the figure, y is the vertical coordinate value of the blade. At this time, the concave surface of blade 1 and the convex surface of blade 2 are windward. Therefore, for blade 1, its concave pressure is greater than the convex pressure. The pressure difference with positive value promotes the wind turbine to work. However, for blade 2, the convex pressure is greater than the concave pressure. The pressure difference with negative value inhibits the wind turbine from working.
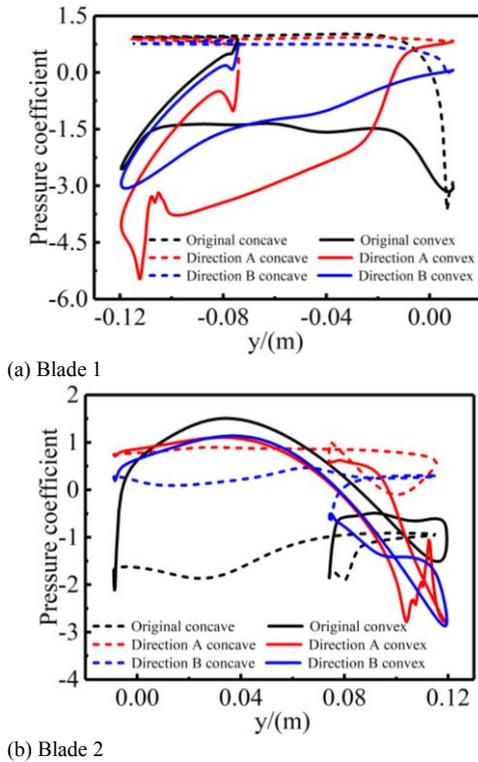

(a) Blade 1

(b) Blade 2

Fig. 14. Surface pressure coefficients on both sides of the blade when *λ*=0.233.

Combining Fig. 14 and Fig. 15, it shows that if the TSR=0.233, on blade 1 in Direction A, the electric field force increases the forward pressure difference, which drives the rise of the output torque on this blade. However, in direction B on blade 1, the electric field force increases the partial pressure difference. Besides, part of the pressure difference is reduced at the same time. The two offset each other and have no significant impact on the blade. Due to the action of the plasma excitation, the electric field forces on blade 2 in both directions reduce the negative pressure difference. Among them, Direction A has a better effect. Moreover, on the blade segment, which is about 0.07<y<0.12, compared with the convex side, the pressure on the concave side is greater, which is consistent with the phenomenon presented in Fig. 9. When the TSR=0.794, the excitation effects of the two plasmas are similar. The
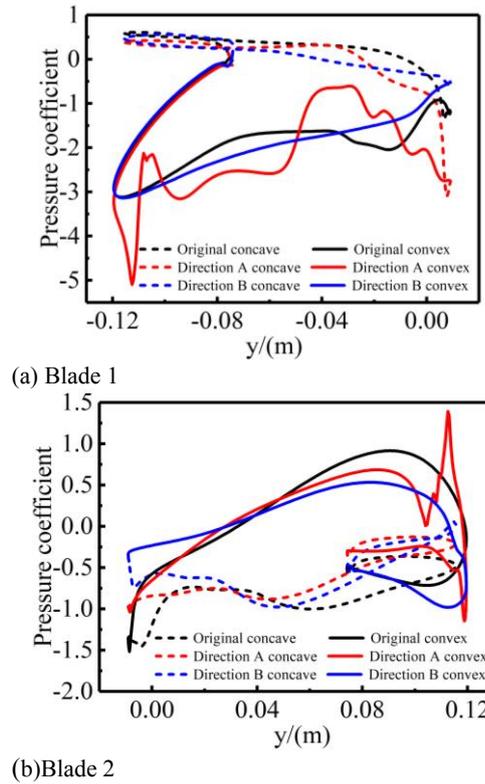

(a) Blade 1

(b)Blade 2

Fig. 15. Surface pressure coefficients on both sides of the blade when *λ*=0.794.

place on blade 1 where the pressure difference increases and the place where the pressure difference decreases offset each other, which results in an insignificant change in positive differential pressure. For blade 2, the electric field force in both directions can reduce the pressure difference that hinders rotation, thereby increasing the output torque.

Therefore, distributed in two directions, the electric field forces can lessen the performance of the Savonius VAWT. However, compared with Direction B, the reasons why the effect of Direction A is better under small TSR are when the wind turbine speed is slow, the high-speed air flow driven by the plasma excitation is greatly affected by the incoming flow; At the moment when the high-speed airflow has an influence on the wind turbine, the direction of the high-speed airflow in direction A coincides with the of the incoming flow direction, and its effect is enhanced; In direction B, the direction of the high-speed airflow is opposite with the incoming flow, and its impact is weakened.

5. CONCLUSION

In this paper, combined with the phenomenological model, the plasma excitation is loaded into three pairs of wind turbine blades through UDF. The influence mechanism of plasma excitation on the overall performance of the Savonius vertical axis wind turbine under different working conditions was studied by numerical simulation method, and the optimal installation position of the plasma excitation was found. At the optimal installation location, the

effects of electric field forces in different directions on the overall performance were compared. The following are the conclusions:

(1) The high-speed jet generated by plasma excitation can change the velocity distribution near the blade, resulting in the change of the pressure field, which changes the magnitude and direction of the pressure difference, and finally affects the overall performance.

(2) The TSR has an important influence on the effect of plasma excitation. When the TSR is small, the air velocity around the blade is also small. The high-speed jet generated by the plasma excitation can easily change the velocity distribution near the blade, thus having a greater impact on the wind turbine. When the TSR is relatively large, the air velocity around the blade is also larger, and the disturbance to the air under the same body force is weakened, so the effect of plasma excitation on the fan is not obvious.

(3) The optimal installation of the plasma excitation is the middle position. When the plasma excitation is loaded at this position, the performance of the wind turbine is always significantly improved. This is because, at this position, the jet generated by the plasma excitation can have a greater impact on the flow field around the blade, and since the middle position is relatively far from the center of rotation, the moment caused by the pressure change on both sides of the blade is also larger.

REFERENCES

Abdollahzadeh, M., J. C. Pascoa and P. J. Oliveira (2018). Comparison of dbd plasma actuators flow control authority in different modes of actuation. *Aerospace Science and Technology*, 78, 183-196.

Adamiak, K. (2020). Quasi-stationary modeling of the dbd plasma flow control around airfoil. *Physics of Fluids* 32(8), 085108.

Baleriola, S., A. Leroy, S. Loyer, P. Devinant and S. Aubrun (2016). Circulation control on a rounded trailing-edge wind turbine airfoil using plasma actuators. *Journal of Physics: Conference Series* 753, 052001.

Belabes, B., A. Youcefi and M. Paraschivoiu (2016). Numerical investigation of savonius wind turbine farms. *Journal of Renewable & Sustainable Energy* 8(5), 333-338.

Bethi, R. V., P. Laws, P. Kumar and S. Mitra (2019). Modified savonius wind turbine for harvesting wind energy from trains moving in tunnels. *Renewable energy* 135, 1056-1063.

Blaabjerg, F. and K. Ma (2017). Wind Energy Systems. *Proceedings of the IEEE* 105(11), 2116-2131.

Chan, C. M., H. L. Bai and D. Q. He (2018). Blade shape optimization of the savonius wind turbine using a genetic algorithm. *Applied Energy* 213, 148-157.

Chen, K., Z. Shi and C. Wei (2020). Influence of DBD on aerodynamic performance of high lift system. *Flight Dynamics* 38(2), 12-16.

Cooney, J. A., C. S. Szlatenyi and N. E. Fine (2016, January). The Development and Demonstration of a Plasma Flow Control System on a 20 kW Wind Turbine. In *54th AIAA Aerospace Sciences Meeting*, San Diego, California, USA.

Dai, K., A. Bergot, C. Liang, W. N. Xiang and Z. Huang (2015). Environmental issues associated with wind energy - A review. *Renewable energy* 75, 911-921.

Fujisawa, N. and F. Gotoh (1994). Experimental study on the aerodynamic performance of a savonius rotor. *Asme Journal of Solar Energy Engineering* 116(3), 148-152.

Gielen, D., F. Boshell, D. Saygin, M. D. Bazilian, N. Wagner and R. Gorini (2019). The role of renewable energy in the global energy transformation - sciencedirect. *Energy Strategy Reviews* 24, 38-50.

Harjanne, A. and J. M. Korhonen (2019). Abandoning the concept of renewable energy. *Energy Policy* 127, 330-340.

Jukes, T. N. (2015). Smart control of a horizontal axis wind turbine using dielectric barrier discharge plasma actuators. *Renewable Energy* 80, 644-654.

Kothe, L. B., S. V. Möller and A. P. Petry (2020). Numerical and experimental study of a helical savonius wind turbine and a comparison with a two-stage savonius turbine. *Renewable Energy* 148, 627-638.

Lee, J. H., Y. T. Lee and H. C. Lim (2016). Effect of twist angle on the performance of savonius wind turbine. *Renewable Energy* 89, 231-244.

Li, G., W. Zhang, Y. Jiang and P. Yang (2019). Experimental investigation of dynamic stall flow control for wind turbine airfoils using a plasma actuator. *Energy* 185, 90-101.

Li, Y. and Y. Wu (2020). Research progress and outlook of flow control and combustion control using plasma actuation, *In Journal of SCIENTIA SINICA Technologica* 50(10), 1252-1273

Lin, J. C., M. Y. Andino, M. G. Alexander, E. A. Whalen, M. A. Spoor, J. T. Tran and I. J. Wygnanski (2016, January). In *54th AIAA Aerospace Sciences Meeting*, San Diego, California, USA.

Lombardi, A. J., P. O. Bowles and T. C. Corke (2013). Closed-Loop Dynamic Stall Control

Using a Plasma Actuator. *AIAA Journal* 51(5),1130-1141.

Mazaheri, K., J. Omidi and K. C. Kiani (2016). Simulation of dbd plasma actuator effect on aerodynamic performance improvement using a modified phenomenological model. *Computers & Fluids* 140, 371-384.

Mikhaylov, A., N. Moiseev, K. Aleshin and T. Burkhardt (2020). Global climate change and greenhouse effect. *Entrepreneurship and Sustainability* 7(4), 2897-2913.

Nie, W. Cheng Y. and Che X. (2012). Recent developments in DBD plasma flow control. *Advances in Mechanics* 42(6), 722-734.

Østergaard, P. A., N. Duic, Y. Noorollahi, H. Mikulcic and S. Kalogirou (2020). Sustainable development using renewable energy technology. *Renewable Energy* 146(2), 2430-2437.

Pescini, E., F. Marra, M. G. De Giorgi, L. Francioso and A. Ficarella (2017). Investigation of the boundary layer characteristics for assessing the dbd plasma actuator control of the separated flow at low reynolds numbers. *Experimental Thermal & Fluid Science* 81, 482-498.

Shmilovich, A., Y. Yadlin and E. A. Whalen (2016, June). Numerical Simulations of an Airplane with an Active Flow Control System. In *8th AIAA Flow Control Conference*, Washington, D.C., USA.

Shyy, W., B. Jayaraman and A. Andersson (2002). Modeling of glow discharge-induced fluid dynamics. *Journal of Applied Physics* 92(11), 6434-6443.

Tahani, M., A. Rabbani, A. Kasaeian, M. Mehrpooya and M. Mirhosseini (2017). Design and numerical investigation of savonius wind turbine with discharge flow directing capability.

Energy 130, 327-338.

Tummala, A., R. K. Velamati, D. K. Sinha, V. Indraja and V. H. Krishna (2016). A review on small scale wind turbines. *Renewable & Sustainable Energy Reviews* 56, 1351-1371.

Veers, P., K. Dykes, E. Lantz, S. Barth, C. L. Bottasso, Carlson, A. Clifton, J. Green, P. Green, H. Holttinen, D. Laird, V. Lehtomäki, J.K. Lundquist, J. Manwell, M. Marquis, C. Meneveau, P. Moriarty, X. Munduate, M. Muskulus, J. Naughton, L. Pao, J. Paquette, J. Peinke, A. Robertson, J.S. Rodrigo, A.M. Sempreviva, J. C. Smith, A. Tuohy and R. Wiser (2019). Grand challenges in the science of wind energy. *Science* 366(443), 1-9.

Vernet, J. A., R. Örlü and P. H. Alfredsson (2015). Separation control by means of plasma actuation on a half cylinder approached by a turbulent boundary layer. *Journal of Wind Engineering & Industrial Aerodynamics* 145, 318-326.

Wang, C. and R. G. Prinn (2010). Potential climatic impacts and reliability of very large-scale wind farms. *Atmospheric chemistry and physics* 10(4), 2053-2061.

Wong, C., L. Wang, W. Ma and Y. Zhou (2020). New Sawtooth Plasma Actuator Configuration and Mechanism Behind Improved Control Performance. *AIAA journal* 58(4), 1881-1886.

Yang, L., J. Li, J. Cai, G. Wang and Z. Zhang (2016). Lift Augmentation Based on Flap. *Journal of Fluids Engineering* 138, 031401.

Zhu, H., C. Li, W. Hao, Q. Ding and W. Yu (2018). Investigation on aerodynamic characteristics of building augmented vertical axis wind turbine. *Journal of Renewable and Sustainable Energy* 10(5), 1-17.